DOI:
10.1039/c8lc01081a

Document Version
Peer reviewed version

Lab on a Chip

Accepted Manuscript

This article can be cited before page numbers have been issued, to do this please use: A. S. Chaurasia and S. Sajjadi, *Lab Chip*, 2019, DOI: 10.1039/C8LC01081A.

This is an Accepted Manuscript, which has been through the Royal Society of Chemistry peer review process and has been accepted for publication.

Accepted Manuscripts are published online shortly after acceptance, before technical editing, formatting and proof reading. Using this free service, authors can make their results available to the community, in citable form, before we publish the edited article. We will replace this Accepted Manuscript with the edited and formatted Advance Article as soon as it is available.

You can find more information about Accepted Manuscripts in the author guidelines.

Please note that technical editing may introduce minor changes to the text and/or graphics, which may alter content. The journal's standard Terms & Conditions and the ethical guidelines, outlined in our author and reviewer resource centre, still apply. In no event shall the Royal Society of Chemistry be held responsible for any errors or omissions in this Accepted Manuscript or any consequences arising from the use of any information it contains.

ROYAL SOCIETY OF CHEMISTRY

rsc.li/loc

View Article Online
DOI: 10.1039/C8LC01081A

Transformable Bubble-filled Alginate Microfibers via Vertical Microfluidics

Ankur Shubhlal Chaurasia[1]† and Shahriar Sajjadi[2]*

[1] ESPCI Paris, 10 Rue Vauquelin, 75231, Paris cedex 05, Paris, France
[2] Department of Physics, King's College London, Strand, London, WC2R 2LS, UK
* shahriar.sajjadi-emami@kcl.ac.uk

Keywords: Vertical microfluidics, alginate microfibers, air-encapsulation, beaded microfibers, threaded capsules, all-aqueous microfibers, anisotropic alginate microparticles, controlled destruction

A novel buoyancy-assisted vertical microfluidic setup is used to fabricate a new class of transformable bubble-filled hydrogel microfibers. A co-axial flow of an aqueous sodium-alginate solution enveloping an air phase was injected into a quiescent aqueous $CaCl_2$ solution, through a vertically-oriented co-axial glass-capillary setup. This induced an instantaneous gelation and produced bubble-filled calcium-alginate fibers. The surface-morphology of resulting fibers was controlled from smooth to wavy by slowing down the gelation kinetics. Advantage of the buoyancy force acting on the fibers by the trapped air bubbles was taken not only to shape the fibers, but to transform them into several other novel hydrogel structures, such as water-filled segmented fibers, beaded microfibers, and threaded capsules. The ultimate transformability was demonstrated by the fibers being allowed to elongate and then undergo a controlled destruction to produce uniform anisotropic micro-particles with wide range of sizes and shapes from frustums to barrel and cylindrical types.

View Article Online
DOI: 10.1039/C8LC01081A

1. Introduction

Microfluidic technologies have recently found significant attention due to their versatilty in production of a wide range of structured materials, among them microfibers are of significant importantce. Microfibers are specific group of advanced materials that are in demand for many applications and particularly for tissue engineering and cell biology. Microfluidic-based spinning techniques have been developed for producing microfibers using different solidification mechnisms.[1] Microfibers can be made out of a simple material, often a polymer or mixture of polymers.[2] Recently, fabrication of hybrid microfibers containing encapsulated materials has also attracted considerable attention for enhancing the performance of fiber-based materials with flexible internal architecture. Gas-filled microfibers are emerging materials that, while share many advantages of gas-filled materials, open up a new range of specific applications. Gas-filled materials are characterized by their light-weight and low-density structures, which make them ideal candidates for energy-efficient transportation purposes.[3] Several naturally-occurring structures also take advantage of their internal gas-filled cavities, such as aquatic plants that use the large air chambers in their leaves to stay afloat.[4] Gas-filled materials with shape and composition being tuned for a variety of applications are artificially constructed using advanced microfluidic techniques. For example, Abbaspourrad et al.[5] demonstrated microfluidic formation of gas-filled micro-capsules with tuneable shell thickness, which were designed to withstand high-pressure environment. Similarly, Wan et al.[6] and Wang et al. [7] employed microfluidic techniques to form gas-filled double emulsions for fabricating hollow bio-compatible hydrogel microspheres and porous microparticles. The encapsulation of a gaseous phase in bio-compatible materials, such as

View Article Online
DOI: 10.1039/C8LC01081A

calcium alginate hydrogel, has also been reported in the literature. Huang et al.[8] fabricated calcium-alginate microbubbles by collecting uniform bubbled-alginate drops in calcium chloride solution. This technique was also exploited by Yang et al.[9] to produce nanoparticles-alginate composite bubbles. More complex biocompatible void structures have also been reported by Wang et al.[10] who produced gas-filled micro-capsules with calcium alginate shell, and packed them together to obtain highly ordered 3D alginate scaffold for advanced tissue engineering applications.

While several investigations have been carried out to form a variety of oil-filled[11-14] or water-filled[15,16] microfibers, reports on the formation of highly structured gas-filled fibers are scarce. Gas-encapsulated or cavity microfibers are useful for providing a temporary source of oxygen for encapsulated cells,[17] and could also act as carriers for delivering gaseous phases, such as nitric oxide, for biomedical applications.[18] Hou et al.[3] reported the generation of bubble-filled silica microfibers, used as filler materials to produce light-weight polydimethylsiloxane (PDMS) composites. Currently, there are very few reports in the literature regarding gas encapsulation in biocompatible microfibers. Kang et al.[17] developed a complex microfluidic approach, integrated with multiple computer-controlled pneumatic valves for encapsulation. They studied encapsulation of variety of materials in alginate microfibers, and briefly considered air-bubble encapsulates. Recently, Tian et al. [19] encapsulated gas in alginate-based composite microfibers to achieve large scale water collection.

The alginate solutions are often lighter than the media they are dispersed in, an aqueous $CaCl_2$ solution. Therefore, there might be a mild tendency for the alginate materials to afloat within a range of compositions. Yoshida and Onoe used this feature to produce microspring microfibers with a variable pitch distance via anisotropic gelation induced by a bevel-tip capillary.[20] The pitch distance varied with time due to a varying buoyancy force acting on the fibers, a feature not observed in horizontal microfluidics.

View Article Online
DOI: 10.1039/C8LC01081A

In most reports cited in the literature, however, horizontal microfluidic devices have been used. We have previously reported the formation of simple drops[21] as well as compound drops[22,23] in vertical microfluidic setups. For core-shell drops in a vertical set up, the buoyancy force stemming from the light shell drop affected the size of the inner core droplets. We also recently reported how the presence of oil encapsulates within microfibers produced in a vertical microfluidic setup can render particular morphology or functions to the fibers.[13,14] In this work, we extend our research on vertical microfluidics to air encapsulates, which can hugely increase the buoyancy force acting on microfibers during their formation. The vertical-orientation of the coaxial glass capillaries allowed the fibers to elongate during their formation, under the influence of buoyancy, and produced morphologies not easily achievable by any other horizontal microfluidic setup. Air-filled microfibers were produced by introduction of a gas-in-alginate flow into a non-confined quiescent aqueous solution of calcium chloride. The resulting fibers moved upwards due to the buoyancy force and were then collected at the surface. The fiber's surface morphology was tuned by controlling the speed of gelation via varying the alginate and calcium chloride concentration. The versatility of these bubble-filled microfibers is demonstrated not only by their wide range of morphologies including all-aqueous fibers with segmented water-cores and uniformly beaded fibers, but by their transformation into a range of anisotropic microparticles.

2. Experimental

2.1 Materials

Sodium alginate and calcium chloride (Sigma Aldrich) were used as received. The middle phase constituted of sodium alginate (1.0 and 4.0 wt%) in the aqueous phase, which was introduced into an aqueous solution of calcium chloride at 1.0 wt%. Tween 20 (Sigma

View Article Online
DOI: 10.1039/C8LC01081A

Aldrich) was used as a surfactant in the aqueous alginate phase to stabilize bubbles. A pressure-regulated flow of filtered and compressed air was used as the inner gas-phase.

2.2 Vertical microfluidic set up

Fig.1a shows the schematic of the *two-step* microfluidic device made for encapsulation of air within the alginate fibers. To fabricate the devices, a circular capillary (ID: 0.10 mm, OD: 0.17 mm) was inserted into a wider capillary (ID: 0.30 mm, OD: 0.40 mm). Both capillaries were used as received without surface treatments. To make the device for the *two-step* encapsulation, the inner tip was placed upstream the outer tip. The air phase was introduced via the inner capillary at a controlled pressure, using a digital pressure gauge (Omega) with a 0.1 psi resolution. The alginate phase was introduced through the interstitial spaces between the two capillaries using a syringe pump (Harvard Apparatus). The coaxially aligned capillary setup was introduced vertically, from the bottom, into a cuvette containing a quiescent aqueous solution of calcium chloride, as shown in Fig.1a. The resulting fibers were collected at the top of the cuvette, facilitated by the buoyancy force exerted by the encapsulated air bubbles. The distance from the capillary tip to the free surface of the $CaCl_2$ solution was kept constant during experiments at 2.80 cm. A high-speed video recording camera (Photron FastCam SA-5-monochrome) was used to record fiber formation.

3. Results and discussion

3.1 Formation of gas-filled microfibers

Gas-filled alginate microfibers were produced using co-axial buoyancy-assisted microfluidic setups, schematics of which are shown in Fig. 1a. The characteristics and applications of such

View Article Online
DOI: 10.1039/C8LC01081A

compound fibers largely depend on their two primary structural features, namely the encapsulate geometry [24] and the fiber (surface) morphology.[25] We first discuss in detail how the air-encapsulate geometry and surface morphology of bubble-filled alginate microfibers can be desirably tuned.

3.2 Tailoring air-encapsulate geometry

Air encapsulates within alginate microfibers can come into two forms; tubular or continuous, divided into two classes, *smooth* and *wavy*, as shown in Fig. 1b, which also illustrates assigned nomenclatures to various fiber dimensions.

3.2.1. Smooth or flat microfibers

A smooth fiber is characterised by a flat surface profile and uniform diameter across the length of the fiber in the wet state. This means that the thickness of the microfiber around the encapsulate (T) is equal to the fiber-only thickness (t). *Tubular* microfibers can also be classified under this category. However, tubular fibers contain a continuous air phase as the inner phase.

The pre-requisite to the formation of smooth fibers is the use of high concentrations of $CaCl_2$ and alginate solutions (i.e., 4.0 wt%) to promote instantaneous gelation at the tip of the capillaries where both solutions first met. The instantaneously gelled shell acts like a solid tube that guides the air flow through itself, forming tubular microfibers. Other conditions for producing tubular microfibers are a high internal phase ratio of air, defined by $\boldsymbol{\varphi_{air}} = Q_{\text{air}}/(Q_{\text{air}} + Q_{\text{alg}})$, to form a continuous air phase together with a sufficiently high Q_{air} to allow a compound core-shell jet to develop at the tip, which gelled to a tubular cavity microfiber. **Fig. 1c** shows a typical tubular microfiber produced at $\varphi_{air} = 0.96$, using the *one-step* microfluidic device configuration in which the inner and outer capillary tips were adjusted at the same level (**Fig. 1.a1).** The width of the shell, which is only a small fraction of the grey wall shown

View Article Online
DOI: 10.1039/C8LC01081A

in Figure 1c, could be controlled within a narrow range by the alginate flow rate. However, the thickness of the fiber was mainly controlled by the capillary tube diameter. These microfibers were quite light and floated on the free surface of water when formed. Note that tubular fibers could be produced using the two-stage protocol too, but within a limited range of flow conditions. In this research, we were mostly interested in segmented fibers due to their versatility.

The *two-step encapsulation approach* was used for producing discontinuous cavities in flat (as well as wavy) microfibers. In the first step, the air phase flowing in the inner capillary was broken into a stream of tiny microbubbles inside the outer capillary by a high drag exerted by the alginate phase flowing within the confinements of the outer capillary. In the second step the stream of air bubbles, engulfed in the alginate phase, was carried by the flow towards the exit orifice of the outer capillary, where the bubbles got locked within the hydrogel fiber formed due to instantaneous reaction between the alginate phase and the calcium ions present in the outer aqueous phase. The gelled shell was strong enough not only to resist the stress applied by growing bubbles at tip, but deform them to an ellipsoidal shape.

The bubble morphology could be tuned by regulating the air pressure and the alginate phase flow rate using the two-state protocol, as seen in **Fig. 1(d-e).** The volumetric flow rate of the inner air phase Q_{air} was controlled by the air pressure. At very low Q_{air}, the dripping regime was dominant, and small air bubbles, which were smaller than the internal diameter of the inner capillary, were formed. An increase in Q_{air}, at a given Q_{alg}, reduced the shear stress on the forming gas bubbles at the inner capillary tip, thereby increased the bubble size (Figure 1d). Furthermore, a high inertia force of the air led to the widening jetting regime being dominant in the outer capillary, leading to the formation of large bubbles that extended inside the outer capillary tube because of the restriction imposed. However, such plugs transformed to spherical bubbles at the outer capillary tip when they were housed inside the alginate fiber.

View Article Online
DOI: 10.1039/C8LC01081A

A decrease in the alginate phase flow rate, reduced the shear stress acting on the bubbles during formation thereby increased their size, as shown in **Fig. 1e**.

The images shown in **Fig. 1e.1** clearly show that fibers having a high φ_{air} (≈0.85) are inclined to be wavy, despite a high $CaCl_2$ concentration used. Apparently, the large surface area developed by big air bubbles around the nodes could not be filled by the low volume of alginate solution being available at high φ_{air}. Paradoxically, at very high φ_{air} (≈0.95), when discrete air bubbles joined to form a continuous inner air phase, the nodes disappeared and the surface of the fibers reverted to smooth.

In addition to varying the alginate phase flow rate and air pressure, the bubble size could also be adjusted by the concentration of the surfactant used in the middle alginate phase. To show this effect, two extreme cases of surfactant concentrations, namely 0 and 1.0 wt% concentration of Tween20, were examined. The surfactant reduced the surface tension between the air phase and the aqueous alginate phase and thus decreased the bubble size (Fig. 1f).

To determine the internal phase ratio φ_{air} in the resulting bubble-filled fibers, the volumetric flow rate of the gas phase (Q_{air}) was determined. We found that Q_{air} increased non-linearly with air pressure via a power relationship (Fig. 1g), which is similar to a previous observation of formation of bubbles in water. [26] More importantly, Q_{air} was so significantly dependent on the alginate phase flow rate (Q_{alg}) that the air phase flow, introduced at a fixed pressure, completely ceased at high Q_{alg} (Fig. 1h). This cessation of the air phase flow at high Q_{alg} is not a result of device malfunction or poor pressure regulation, but due to an increased back-pressure which drives the air stream backwards into the inner capillary, as explained previously in a similar observation.[27] This mechanism was also utilised by Sullivan et al.[28] for getting rid of bubbles from microchannels without the need to reduce the air pressure. The internal air phase ratio in the collected fibers could be appropriately tuned via varying the air

View Article Online
DOI: 10.1039/C8LC01081A

pressure and Q_{alg}. Fig. 1i shows that fibers with a high internal air ratio could be obtained at increased air pressure and reduced Q_{alg}. Fibers at very high φ_{air} contain elliptical air capsules, and tend to be wavy.

3.2.2. *Wavy microfibers:*

A wavy morphology is identified with a significant variations in the diameter along the fiber length, indicated by $T > t$ (Fig. 1b). Wavy fibers, compared to smooth fibers, have a higher surface roughness due to the non-uniform surface area across their length. They are often useful for applications that require high interfacial area, such as enhanced water collection at the bulged surfaces along the fiber length at regular intervals.[25] Discrete encapsulates were used to impart wavy morphology to the fibers when the gelling condition was mild. We note that the segmented fibers are eventually wavy when they are in dried state, due to the alginate phase shrinking significantly and the trapped discrete air-encapsulates not changing in size upon drying. However, segmented fibers may have smooth surface morphology (Fig. 1b) in the wet state. In this work we only apply the term "wavy" to wet microfibers resulting from the fabrication process.

The surface roughness or waviness of fibers was mainly controlled by the gelling dynamics of the alginate phase, which were reliant on the alginate and calcium chloride concentrations. A decrease in calcium chloride or alginate concentration slowed down the gelation kinetics and formed a soft and lowly cross-linked shell around the encapsulated bubbles. Such a shell was easily deformed in the radial direction by large bubble encapsulates and transformed from a smooth wall to a wavy one, as illustrated in Fig. 1j. Fig. 1(k-m) represents few examples of wavy microfibers formed using a low $CaCl_2$ concentration of 1 wt%. In addition to the primary role of $CaCl_2$ concentration, which will be discussed later in more detail, the alginate concentration and the flow conditions are also important in shaping the wavy fibers.

Specifically, the alginate concentration and the alginate phase flow rate (Q_{alg}) should be decreased, and the air pressure be increased to make the fiber's surface wavier, as shown in Fig. 1k, 1l, and 1m, respectively. This means fibers with a higher φ_{air} and deformable gelling phase are more likely to be wavy. An increase in the air pressure produced larger bubbles, due to the associated decrease in the shear stress applied. This boosted the buoyancy force acting on the fibers, which further stretched the fibers and allowed a wavy morphology to emerge. A reduced Q_{alg} also increased the bubble size, for the same reason, and allowed air encapsulates to deform the fiber.

As a general principle, the fiber thickness between the consecutive encapsulates could be reduced by lowering the alginate phase flow rate, similar to the trend observed for decreasing thickness of simple alginate fibers.[24] However, this approach suffered from an outer tip blockage at low Q_{alg} when a high $CaCl_2$ concentration was used. This was due to a fast diffusion of Ca+ ions into the slow moving alginate phase, and a fast gelation of the alginate phase inside the outer capillary near the tip. The fabrication of wavy fibers at significantly high φ_{air} ($Q_{alg} \approx 1$ ml/h, Fig. 1l) was only possible at a low [$CaCl_2$], without the risk of inner capillary tip being blocked.

3.3 Transformability of Bubble-filled Alginate Microfibers

Air-filled microfibers are in their early stages of development, and while they seem to have significant potential applications, as outlined in the introduction, their wider applications have not been identified yet. Here, we describe a few examples of how bubble-filled fibers can be used as intermediates to fabricate complex microfibers and microstructures in wet as well as in dried states.

3.3.1. Fine tuning air-filled alginate microfibers via restrained dehydration

View Article Online
DOI: 10.1039/C8LC01081A

Compound alginate fibers are widely used in dried state in different formats, such as free-standing fibers and non-woven pads. The conventional method to alter fiber morphology is to adopt appropriate protocols during their fabrication. The morphology of hybrid hydrogel fibers, however, may change so drastically upon dehydration that it may even cause their shell to fracture.[13]

We studied dehydration of air-filled fibers as a means to further tune their surface morphology. Fibers are usually dehydrated in air in an unrestrained condition, where they can respond to any alteration in their morphology caused by radial and axial shrinkage. We consider two drying protocols, unrestrained or conventional drying and restrained drying, as schematically presented in Fig. 2a and Fig. 2b, respectively.

A typical conventional (unrestrained) drying of an alginate fiber completely suspended in air causes considerable shrinkage across its two axis, namely length and diameter, as observed in Fig. 2a2 In this case, the shrinkage across the length of the resulting dried fiber (25.2% shrinkage) was found to be nearly similar to that across the radial length around the air encapsulates (29% shrinkage).

In the restrained process, the fiber was fixed at both ends so that no axial shrinkage was possible. In order to monitor the evolution of fibers morphology with time, however, we developed a similar method by which the fiber was fixed across its axis. The fiber was placed on a dry and flat (glass) surface for dehydration, instead of being fixed in air. The fiber wet the hydrophilic glass surface at its bulged points, thus securely pinned down on the surface (Fig. 2b2) and was then allowed to dry at room temperature. The restrained drying did not allow axial variation (0% shrinkage) in the fiber, and the fiber retained its full length even after dehydration, as observed in Fig. 2b2. To compensate for the lack of axial shrinkage, however, the fiber underwent more radial shrinkage (39% shrinkage) than in the case of unrestrained drying. This deformed the spherical encapsulate, without rupturing the shell, and

View Article Online
DOI: 10.1039/C9LC01081A

transformed it into an ellipsoidal one. This mechanism worked well for both smooth and wavy fibers in wet state.

Fig. 1e1 shows that an ellipsoidal air-encapsulate morphology can only be achieved at high φ_{air} under normal conditions. The post-fabrication restrained drying process demonstrated in Fig. 2 introduces an interesting way to produce ellipsoidal encapsulate morphology even at low φ_{air}, thus providing more opportunities to fabricate a wide range of fibers under more flexible conditions.

3.3.2. All aqueous-phase microfibers via 2-stage gelation/diffusion

Currently there is no methodology available to produce alginate fibers with segmented aqueous encapsulates. This is because the injection of an aqueous phase into an aqueous alginate microfiber always results in a tubular or irregular encapsulation due to the ultra-low interfacial tension between the alginate and the inner water phase.[15,16] While tubular fibers may have high encapsulation volume, they suffer from a high *spillage ratio*, that is, fibers with tubular encapsulate geometry are highly susceptible to complete core-loss after an accidental rupture, especially during their handling. Fibers with segmented encapsulates, on the other hand, are highly robust against core-loss due to the discontinuous encapsulation, for all types of encapsulated phases including gaseous, non-aqueous and aqueous. In this section, we demonstrate how the air-filled microfibers can be transformed into all-aqueous fibers.

To produce alginate fibers with segmented water cores, the air bubbles within a preformed alginate microfibers were allowed to dissolve out in water (Fig. 3a), during which the core space was simultaneously refilled by water from the continuous phase, as can be observed in Fig. 3b. To enhance the diffusion/dissolution of the trapped air bubbles in the aqueous phase, the gelation of the hydrogel shell was interrupted prematurely by removing the fiber from the calcium chloride solution immediately after its formation, and immersing it in a bath of pure water. The air bubbles slowly dissolved away into the pure water, for example in ~30 min for

View Article Online
DOI: 10.1039/C8LC01081A

the fiber shown in Fig. 3b1. The floating air-encapsulated fiber sank when it was completely refilled with the aqueous solution. To confirm that the dissolution of air bubbles in water occurred because of incomplete alginate gelation in the 1st stage, the bubble-filled microfibers, produced under normal conditions to complete gelation, were observed in a calcium chloride solution for several hours after their formation, but they did not show any sign of air-core dissolution.

This 2-stage gelation approach can be utilised for fabrication of fibers with segmented aqueous cores containing drugs or other ingredients for controlled release. The all-water fibers can be placed in the aqueous solution of the desired active materials to allow their incorporation into the fibers. Large molecules such as long polymer chains may not be able to pass through the cross-linked alginate gel matrix to be encapsulated. However, the range of application can be extended by creating a lowly crosslinked macro porous hydrogel matrix for dissolution purposes via altering the alginate and calcium chloride concentrations, which can tune the pore size between a few nanometres to tens of micrometres.[29] After encapsulation of desired water-soluble ingredients, the fibers can be immersed in an aqueous solution containing the required concentration of $CaCl_2$ for completing the 2nd stage gelation and imposing the desired release kinetics of the ingredients.

3.3.3. Beaded microfibers via dehydration of all-aqueous fibers

Beaded-alginate fibers constitute large lumps of alginate gel across their length at constant intervals. Recent investigations have shown that the heterogeneous beaded-fiber structure enables the non-woven fiber mesh to achieve enhanced de-wetting properties due to the increased surface roughness.[30,31] Formation of beads by using gyration under pressure has been reported.[32] In electro-spinning manufacturing techniques of beaded fibers, the beads-on-string structure is obtained by tuning the fluid physical properties such as surface tension and viscosity,[33,34] but this also makes the spacing between the beads difficult to control. In wet

View Article Online
DOI: 10.1039/C8LC01081A

spinning manufacturing approaches, beads are formed by inducing interfacial instabilities.[35] But similarly these methods lack precision, accuracy, and flexibility to controllably tune the bead size and frequency.

We introduce a stepwise approach to fabricate beaded calcium alginate microfibers with uniform and tunable bead structures. The approach requires slow drying of water-filled fibers formed via the 2-stage gelation. Firstly, we formed alginate microfibers with uniformly spaced air cavities and then replaced the air with water (Fig. 4a1), as discussed in the previous section. The fibers, which had water-core segments, were then dehydrated while completely swollen with water. After their complete dehydration, the fibers structure morphed into beaded alginate microfibers with uniformly spaced beads, as schematically presented in Fig. 4a1-4a3, and observed in Fig. 4b. The water inside the cores compensated the water lost by the alginate shell, kept it plasticised, and allowed it collapse as the cores shrank, due to evaporation. This continued until the cores became void of water, and the shell around them completely collapsed to form thin threads. In contrast, the fiber threads produced thick beads because of having a large alginate gel content when dried. Note that conventional drying of the air-filled fibers straightaway, before replacing the air by water, led to the formation of thin fibers containing large air capsules. The advantages of this approach are that all beads were identical, and the inter-bead distance and size of the beads could be precisely and accurately tuned. The inter-bead distance is geometrically equal to the axial length of the entrapped bubble D, which increased with increasing φ_{air}. The bead size could be increased by decreasing φ_{air}, due to the associated increase in alginate volume present between the adjacent bubbles (Fig. 4c). Furthermore, we anticipate this approach can be extended to achieve more complex and desirable beaded morphologies with exquisite precision, such as asymmetric alternating small and large bead structures via asymmetric encapsulation[13] of parallel bubble streams.

View Article Online
DOI: 10.1039/C8LC01081A

2.3.4. Threaded microcapsules via controlled-elongation of fibers

Capsules are being used for a wide range of applications such as extraction of pollutants, and encapsulation or controlled release of drugs. For some applications, the difficulty in collection and disposal of the capsules or the regeneration of capsules is the main obstacle to their further developments**.** The formation of large capsules connected via long thin threads via horizontal microfluidics is hampered by difficulties involved in the adjustment of the flow rates. Small capsules, can be easily produced at low φ_{air}, but they are contained in thick fibres. In contrast, large capsules can be produced at high φ_{air}, but for the same reason they are in close proximity. The buoyancy assisted mechanism operating in the vertical microfluidic setup allows to produce large capsules connected by a long thin thread. In a previous section we showed that each cavity across the air-filled fibers can be easily replaced by water. This suggests that these connected capsules can potentially be used as threaded capsules if the thickness of the microfiber threads can be reasonably tuned. The presence of a thread connecting the capsules helps to collect and dispose/regenerate such capsules more easily.

Benchmark experiments were carried out to find the stretchability of a passive fiber (i.e., the alginate phase) in the absence of gelation reaction by buoyancy force exerted by the rising bubbles. **Fig. 5**a shows that the alginate fiber continually elongated by the rising bubbles until eventually was ruptured across its threads at some height. A lower alginate concentration decreased the strength of the passive fiber and brought the rupture point to a lower height. The stretching was supressed in the presence of $CaCl_2$. Another benchmark experiment was carried out to find the minimum $CaCl_2$ concentration required to stop the rupture of the fiber. The $CaCl_2$ concentration was found to be 0.05 wt% for [Alg] = 4.0 wt%.

The elongation of fibers and its nomenclature are schematically presented in Fig. 5b. A series of time-evolution micrographs of fibers stretching are shown in Fig. 5c, for the fiber produced at [$CaCl_2$] = 1.0 wt% at the conditions of Fig. 1m (P = 0.2 psi). Within the *stretching zone*, the alginate thread elongated from its initial length (z_i) to its final stretched length (z_s),

View Article Online
DOI: 10.1039/C8LC01081A

accompanied by a continuous thinning from the initial diameter (t_i) to the final stretched diameter (t_s). The alginate fiber elongated during gelation by the buoyancy force acting on the fiber, which emerged from the presence of air pockets in the fiber. The buoyancy force caused the fiber diameter (t) to reduce as the fiber ascended in the medium. The fiber elongation can be better discussed in terms of two consecutive air bubbles, lagging and leading bubbles, with a varying thread length connecting them (Fig. 5c). We note that the lagging bubble is still in the outer capillary while the leading bubble already introduced to the $CaCl_2$ solution in the cuvette. It can be noticed that the distance between consecutive air bubbles inside the capillary remained constant (shown with blue lines), but increased significantly with time (Fig. 5c, green lines) as the leading bubble distanced the tip under the influence of buoyancy when the *lagging* bubble was still inside the outer capillary. For all fibers made using the $CaCl_2$ concentration of 1.0 wt%, the stretching of the thread length (z) stopped before the lagging bubble exited the outer capillary, indicating that the duration of stretching was shorter than the consecutive bubble formation time. This means no further stretching occurred after an emerging lagging bubble exited the outer capillary tip (Fig. 5c, 48-56 ms). This is confirmed by an identical stretched alginate thread across the fiber length in Fig. 1m (0.2 psi).

To further increase the length of the thread connecting capsules, the stretching was extended beyond the exit of lagging bubble. This was carried out in two ways: a) by using a lower $CaCl_2$ concentrations in the outer aqueous phase (<< 1wt%) (Fig. 5d), which slowed down the rate of gelation and thus made the alginate (thread) phase more deformable, and b) by increasing the air pressure (Fig. 5e), which increased the buoyancy force acting on the threads by forming larger bubbles. In the former case, one should note that a decrease in the concentration of $CaCl_2$ reduced the density difference and thus the buoyancy force acting on the fiber. However, this does not appear to be critical due to a large difference between the densities of water and air. These mechanisms created an extended *stretching zone* as indicated

View Article Online
DOI: 10.1039/C8LC01081A

by the red lines in Fig. 5d and 5e. Beyond stretching zone, further elongation ceased as the gelling fiber achieved sufficient strength to withstand the operative tensile force.

The extents of fiber elongation and thinning are depicted in Fig. 5d2-d3 and Fig. 5e2-e3 for the fibers formed via slow-gelation and buoyancy-driven approaches, respectively. A comparative analysis of the fiber thinning reveals that slowing down the gelation kinetics (Fig. 5d2-d3) is far more efficient approach than the enhanced buoyancy-driven elongation (Fig. 5e2-e3). This is partly due to the fact that increasing the air pressure acts counteractively and reduces the length of threads, which then makes it too difficult to achieve long stretched threads.

The slow-gelation approach allowed threads with $t_s \sim 20$ μm to form with the maximum thinning ratio of t_i/t_s=10, as seen in Fig. 5d2. The kinetic approach also provided a maximum elongation ratio of z_s/z_i=100 (compare Fig. 5d3 and Fig. 5e3) due to the presence of a sufficient volume of alginate phase in the threads for longer stretching, which was not possible with increasing the air pressure as it would reduce the alginate phase ratio ($\varphi_{alg} = 1-\varphi_{air}$) and limit the thread volume.

We were mostly interested in the steady-state production of fibers, which was achieved when fibers reached the free surface. This ensured the distance between the capsules across the fibers remained constant. The magnitude of the buoyancy force acting on a deformable fiber is beyond the scope of this research, but varies with the length of an emerging fiber above the tip, from the edge of the tip to the free surface, and the frequency and size of bubbles. Fig. 5c2 shows collection of an emerging fiber at the free surface.

3.3.5. Anisotropic microparticles via controlled destruction of fibers

Fabrication of non-spherical microparticles has recently received considerable attention due to their anisotropic properties and high surface area. Such microparticles have been

View Article Online
DOI: 10.1039/C8LC01081A

demonstrated to be useful for functional enhancements in different applications, such as drug delivery[36], controlled optical light scattering in the form of microlenses[37] and as building blocks for complex assemblies.[38,39] Microparticles made of biocompatible hydrogels in particular, such as calcium alginate microparticles, are ideal for drug administration[40-42] and cell encapsulation[43], where the anisotropic shapes of these microparticles can significantly enhance their performance, due to the increased surface area and raise the possibility of achieving higher packing.

Broadly, the manufacturing of anisotropic particles can be divided into two categories. One approach uses masking or templating to fabricate particles with exotic designs. The continuous-flow lithography[44] and the stop-flow lithography[45,46] techniques belong to this category. They have been applied on single-phase fast-curing (acrylate) monomers to give desired shapes to the polymer microparticles formed. In the masking technique, the particles shape is fixed by designing a transparency mask installed on the UV source to which the flowing monomer phase is exposed. An off-chip suspension photo-polymerization approach has also been reported to produce anisotropic polymeric microparticles.[47] Qiu et al.[43] used a soft-lithography approach to produce hydrogel microparticles with prefixed shapes and sizes, based on the shape of the etched micro-wells on a PDMS template, which were filled with alginate phase and later introduced into a calcium chloride bath for gelation. However, this latter method cannot be used for a continuous production of hydrogel microparticles.

The other category of research is focused on using process and formulation variables to produce particles with different shapes. Liu et al.[47] demonstrated the formation of calcium-alginate microparticles with variety of shapes such as plugs, discs, rods and threads via fusing in a 2D PDMS microfluidic device. Several other studies[48-52] also employed PDMS as well as glass-capillary based microfluidic devices to fabricate tadpole-shaped calcium-alginate microparticles by altering various parameters including calcium chloride concentration in the continuous phase, viscosity and stirring mode of the continuous phase, alginate concentration,

View Article Online
DOI: 10.1039/C8LC01081A

interfacial tension, initial droplet size, collecting height, as well as the impact velocity at the crosslinking interface.

In all fabrication methods described above, the morphology of particles is shaped via either designing a well-defined template and a UV mask, or by constructive alteration in the morphology of a time varying template which eventually takes up the desired morphology. In this part, we introduce a novel destructive method in which the shape of particles emerges from a controlled degradation of microfibers. This facile air-assisted microfluidic approach can form highly uniform calcium-alginate microparticles and microfibers with a wide range of shapes and surface-to-volume ratios. A similar concept, though in a different context, has been previously used to transform a high-viscosity jet, which was difficult to rupture, to unstable core-shell drops, which produced uniform drops after the escape of inner cores.[53]

Encapsulates or air pockets across a fiber can be seen as joints connecting many threads. If these joints are ruptured, via the release of encapsulate, a fiber can be reduced to several long or short fibers, rods or particles whose shape depends on the fabrication conditions. A schematic of the destructive fabrication method is shown in Fig. 6a. The joints can be ruptured by adjusting the conditions to allow the encapsulated air bubbles to escape out of the microfibers.

Air-Alginate compound jets were found to disintegrate soon after they were injected into an aqueous solution in the absence of gelation reaction, in particular when the bubbles were large, due to the buoyancy force exerted by fast rising bubbles (Fig. 5a). To produce structured materails, the rupture of the thread should be avoided. The presence of small amount of $CaCl_2$ was found to be sufficient to impart resistance to the threads against rupture. The slow gelation kinetics, however, did not stop the escape of bubbles, but delayed it so that an emerging fiber could be stretched to some extent by rising bubbles before the bubbles could escape. The use of surfactant in the alginate phase reduced the surface tension and

facilitated stretching of the fibers, while giving partial stability to the bubbles during stretching. The eventual escape of the bubbles, which could not be tightly kept in by the soft gelling phase, at some height above the capillary tip then led to the formation of equally-cut ultra-thin microfibers (Fig 6.a). The technique is similar to the one described for fabrication of threaded capsules. However, [$CaCl_2$] should be smaller than the experimentally found critical value 0.05wt% to avoid fast gelation and entrapment of the bubbles. To highlight the significance of this energy-saving technique for the fabrication of ultrathin fibers, we note that a capillary of 300 μm in diameter was used in our experiments. The pressure drop in laminar flow scales with channel diameter as d^{-4}, as classically defined by the Hagen-Poiseuille relationship. This suggests the fabrication of fibers with 20 μm diameter, as obtained in this work for a typical experimental condition, using micro-channels of the same size will be 5×10^4 times more energy intensive than the method proposed here. This is an astronomical reduction in the energy consumption for producing ultra-thin microfibers via passive wet-spinning, where the fiber thickness is usually governed by the orifice dimension.[54] The buoyancy-assisted passive spinning could also be an alternative for the energy-intensive electro-spinning techniques for producing ultra-thin fibers.[55]

Interesting morphologies can emerge in particular at high air-phase ratios when the bubbles escape soon after they are housed in the fibers. The concentration of surfactant in the alginate phase should be minimized to limit the stretching of the fibers by allowing the bubbles to escape quickly. To capture and freeze the dynamic morphologies of the alginate phase after bubble escape to produce uniform microparticles, an appropriate concentration of $CaCl_2$ should be used to enhance gelation kinetics. Both conditions limited the elongation of the fibers and merely conserved the shape of the fibers prior to their disintegration. There are some precautions to be made too. Formation of small bubbles, for example, should be avoided as this could lead to permanent encapsulation of the bubbles. Furthermore, the presence of even small amount of surfactant in the alginate phase could lead to a permanent encapsulation

View Article Online
DOI: 10.1039/C8LC01081A

of bubbles. To favour the escape of the bubbles and expedite the disintegration of fibers, we did not use surfactant in the alginate phase. This also helped to generate large bubbles due to the associated increase in the interfacial tension. The shape of the microparticles resulting from fibers disintegration could be mainly manipulated by altering the alginate and air phase flow rates, and to a lesser extent by changing concentrations of the reactants. The evolution of the morphology of the microparticles can be best discussed in terms of the internal air phase ratio φ_{air} that takes into account relative changes in Q_{air} and Q_{alg}.

Fig. 6b describes the conditions under which short micro rods were produced. At very low internal phase ratios, the air bubbles were small and did not succeed in escaping from the fibers. At φ_{air} = 5%, air bubbles with a diameter almost equal to the fiber width were formed. These bubbles could manage to cut the fibers into equal *short cylindrical fibers* or *rods*. The air-assisted fiber cutting in the suggested microfluidic approach eliminates the need for mechanical cutting usually required in other fabrication methods. The length of the rods could be tuned by varying φ_{air} (i,e., P); increasing φ_{air} resulted in shorter rods being formed because of the shorter clearance between the bubbles (Fig. 6b.3). The size of air bubbles within the fibers showed insignificant change with increasing air pressure within 0.5-0.7 psi.

Fig. 6b.4 shows that by increasing φ_{air}, one can form a row of bubbles in a close proximity within the jet of alginate solution. A controlled destruction of such fibers led to the formation of particles with the shape of "⧓". The length and thickness of ⧓ particles could be tailored by playing with φ_{air}. The minimum thickness of ⧓ particles can be expected at $\varphi_{cr} \approx 66.6\%$ when a chain of bubbles is formed in a flat fiber jet with the same diameter.

As the internal phase ratio of air φ_{air} increased beyond this critical phase ratio, the smooth cylindrical shape of the fiber jets could not be maintained anymore due to a significant increase in the size of the air bubbles, as previously explained. The increase in the size of bubbles, combined with a lower volume of the alginate phase available at high φ_{air}, produced wavy fibers with short thin threads, in the form of *frustum,* connecting the bubbles. The

View Article Online
DOI: 10.1039/C8LC01081A

threads connecting air encapsulates were quite symmetric in the presence of surfactant (see Fig. 1.b2, 1.e1 and 1.k-m). The asymmetric *frustum* shape of the threads connecting the air bubbles stems from dewetting of the air bubbles by the alginate phase, due to a high surface tension in the absence of surfactant, and the resistance of the threads to deform, as seen in Fig. 6c. Fig. 6b5 shows that the breakdown of the conical frustum threads formed at $\varphi_{air} \approx 0.75$ resulted in the formation of uniform calcium-alginate frustum microparticles. The dimension of the frustum microparticles could be further adjusted by an increase in φ_{air}. Fig. 6b6 shows that at $\varphi_{air} \approx 0.90$, the threads connecting the bubbles were more pact, with a wider difference between the base and top radii, thin frustum with large slant height, making it similar to a *plate*-type particles. The conical frustums had corrugated or wrinkled surface, like cupcakes, formed because of the capillary forces applied by escaping bubbles on the soft alginate substrate.[56] This is an interesting features, clearly observed from the optical and SEM images provided in Fig. 6d, which can serve to increase the surface area of particles significantly.

View Article Online
DOI: 10.1039/C8LC01081A

While there is a wide range of possibilities to tailor make the shape and size of anisotropic particles, we limit our discussion to two more examples. The use of a lower concentration of alginate made the fiber more deformable at the tip and allowed for interesting morphologies to emerge. Fig. 6b7 shows that at [Alg] = 2.0 wt%, where the viscosity of the gel phase was relatively small and the gelation rate highly reduced, cylindrical particles with concave surface was produced due to outward deformation of the threads during crosslinking; *barrel*-type particles. A close look at the microfluidic formation of threads in Fig. 6c reveals that the frustum alginate threads elongated to some extent before air bubbles ruptured. Fig. 6b8 shows anisotropic frustum microparticles formed at $\varphi_{air} \approx 0.75$, but using a higher calcium concentration. A higher concentration of $CaCl_2$ restricted further deformation of threads under the influence of the buoyancy force as they emerged at the tip. This minimized the distance between the bubbles thus producing thinner frustums.

Overall, the structural breakdown of the alginate microfiber resulted in the formation of uniform calcium-alginate microparticles with different shapes including cylindrical rods, conical frustums, barrels and plates having extremely high surface-to-volume ratio, as shown in Fig. 6. The simplicity of this technique, coupled with the wide range of possible shape-modification and ease of scalability, makes it attractive for different applications such as biomedical therapeutics and the encapsulation of biomaterials.

4. Conclusion

A facile and novel buoyancy-assisted microfluidic technique was introduced for a continuous fabrication of air-filled alginate microfibers with tuneable encapsulate and fiber morphology. A wide range of segmented bubble size and geometry, including

spherical, ellipsoidal and plugs was produced by altering the air and alginate phase flow conditions. The surface morphology of the fibers was turned from smooth to wavy by slowing down the gelation kinetics via decreasing calcium chloride concentration.

The bubble-filled alginate microfibers were morphed to create a range of new fiber structures, including all-aqueous alginate fibers with segmented water-cores and tunable beaded microfibers and threaded capsules. Ultra-thin alginate microfibers (~20 μm diameter) were produced by exploiting the buoyancy force acting on the fibers by the trapped bubbles, and stretching them under slow gelation conditions. To obtain all-aqueous alginate fibers with segmented water-cores, the entrapped air bubbles were allowed to dissolve out into the outer water through partially gelled shells, while the outer water filled the cores. The fibers with segmented water-cores were dehydrated to obtain alginate microfibers with uniformly distanced monodisperse beads, whose frequency, size and shape were easily controlled by altering the bubble encapsulate geometry. Lastly and more importantly, the microfibers were disintegrated in a controlled manner to capture the emerging morphologies between escaping bubbles and produce a wide range of uniform

anisotropic micro-particles. The upper-limit thickness of the fibers was controlled by the inner diameter of the outer capillary used, which was fixed at 300 μm in this work. Elongated fibers as thin as 20 μm was produced, however, there is a potential to further reduce the thickness of fibers. Air capsules ranged from twice of the capillary diameter used to a fraction of it. Anisotropic particles with the characteristic size in the order of the capillary tube diameter were produced. The diameter of the bottom base of the conical frustum microparticles was mainly controlled by the inner diameter of the outer capillary used, but their heights could be adjusted by altering the concentration of reactants as well as their flow rates. The process can be easily scaled out by using equally distanced multiple capillaries.

Acknowledgements

We acknowledge the use made of Photron FastCam SA-5 (monochrome) high-speed video recording system, which was borrowed from the EPSRC (Engineering and Physical Sciences and Research Council) Engineering Instrument Pool.

Received: ((will be filled in by the editorial staff))
Revised: ((will be filled in by the editorial staff))
Published online: ((will be filled in by the editorial staff))

References

1 Y. Jun, E, Kang, S. Chae, S.H, Lee, Microfluidic Spinning of Micro- and Nano-scale Fibers for Tissue Engineering. *Lab Chip* 2014, **14**, 2145-2160.

2 P. L. Heseltine, J. Ahmed, M. Edirisinghe, Developments in Pressurized Gyration for the Mass Production of Polymeric Fibers. *Macromol. Mat. Eng.* 2018, **303**, no.1800218.

3 L. Hou, H. Jiang, D. Lee, Bubble-filled Silica Microfibers from Multiphasic Flows for Lightweight Composite Fabrication. *Chem. Eng. J.* 2016, **288**, 539-545.

DOI: 10.1039/C8LC01081A

4 H.B. Sifton, Air-Space Tissue in Plants. *Bot. Rev.* 1945, **11**, 2, 108-143.

5 A. Abbaspourrad, W.J. Duncanson, N. Lebedeva, S. Kim, A.P. Zhushma, S.S. Datta, P.A. Dayton, S.S. Sheiko, M. Rubinstein, D.A. Weitz, Microfluidic Fabrication of Stable Gas-Filled Microcapsules for Acoustic Contrast Enhancement. *Langmuir* 2013, **29**, 40, 12352-12357.

6 J. Wan, A. Bick, M. Sullivan, H.A. Stone, Controllable Microfluidic Production of Microbubbles in Water-in-Oil Emulsions and the Formation of Porous Microparticles. *Adv. Mater.* 2008, **20**, 17, 3314-3318.

7 W. Wang, R. Chen, J. Xu, Y. Wang, G. Luo, One-step Microfluidic Approach for Controllable Production of Gas-in-Water-in-Oil (G/W/O) Double Emulsions and Hollow Hydrogel Microspheres. *RSC Adv.* 2014, 4, **32**, 16444-16448.

8 K. Huang, Y. Lin, W. Chang, Y. Wang, C. Yang, A Facile Fabrication of Alginate Microbubbles Using a Gas Foaming Reaction. *Molecules* 2013, 18, 8, 9594-9602.

9 C. Yang, W. Wang, A,M, Grumezescu, K. Huang, Y. Lin, One-step Synthesis of Platinum Nanoparticles Loaded in Alginate Bubbles. *Nanoscale Res. Lett.* 2014, **9**, 277.

10 C. Wang, K. Yang, K. Lin, H. Liu, F. Lin, A Highly Organized Three-dimensional Alginate Scaffold for Cartilage Tissue Engineering Prepared by Microfluidic Technology. *Biomaterials* 2011, 32, 29, 7118-7126.

11 Y. Yu, H. Wen, J. Ma, S. Lykkemark, H. Xu, J. Qin, Flexible Fabrication of Biomimetic Bamboo-like Hybrid Microfibers. *Adv. Mater.* 2014, 26, 16, 2494-2499.

2 E. Um, J.K. Nunes, T. Pico, H.A. Stone, Multicompartment Microfibers: Fabrication and Selective Dissolution of Composite Droplet-in-Fiber Structures. *J. Mater. Chem. B* 2014, 2, 45, 7866-7871.

13 A.S. Chaurasia, S. Sajjadi, Flexible Asymmetric Encapsulation for Dehydration-Responsive Hybrid Microfibers. *Small* 2016, 12, 30, 4146-4155.

14 A.S. Chaurasia, F. Jahanzad S. Sajjadi,Flexible Microfluidic Fabrication of Oil-Encapsulated Alginate Microfibers. *Chem. Eng. J.* 2016, **308**, 1090-1097.

5 Y. Cheng, F. Zheng, J. Lu, L. Shang, Z. Xie, Y. Zhao, Y. Chen, Z. Gu, Bioinspired Multicompartmental Microfibers from Microfluidics. *Adv. Mater.* 2014, 26, 30, 5184-5190.

6 Y. Cheng, Y. Yu, F. Fu, J. Wang, L. Shang, Z. Gu, Y. Zhao, Controlled Fabrication of Bioactive Microfibers for Creating Tissue Constructs using Microfluidic Techniques. *ACS Appl. Mater. Interfaces* 2016, 8, 2, 1080-1086.

7 E. Kang, G.S. Jeong, Y.Y. Choi, K.H. Lee, A. Khademhosseini, S. Lee, Digitally Tunable Physicochemical Coding of Material Composition and Topography in Continuous Microfibers. *Nat. Mater.* 2011, 10, 11, 877-883.

8 A.B. Seabra, N. Duran, Nitric Oxide-Releasing Vehicles for Biomedical Applications. *J. Mater. Chem.* 2010, 20, 9, 1624-1637.

9 Y. Tian, P. Zhu, X. Tang, C. Zhou, J. Wang, T. Kong, M. Xu, L. Wang, Large-scale water collection of bioinspired cavity-microfibers. *Nat. Commun.* 2017, 26, 30, 5184-5190.

20 K. Yoshida, H. Onoe, Functionalized core-shell hydrogel microsprings by anisotropic gelation with bevel-tip capillary. Scientific Reports 2017, **7**, 45987-45987.

21 A.S. Chaurasia, D.N. Josephides, S. Sajjadi, Buoyancy-driven drop generation in microchannel revisited. Microfluid. Nanofluid. 2015, **18**, 943–953

22 A.S. Chaurasia, S. Sajjadi, Millimetric core-shell drops via buoyancy assisted non-confined microfluidics, *Chem. Eng. Sci.* 2015, **129**, 260-270

23 A.S. Chaurasia, D.N. Josephides, S. Sajjadi, Large Ultrathin Shelled Drops Produced via Non-Confined Microfluidics, *Chemphyschem* 2015, **16**, 403-411.

24 X. He, W. Wang, K. Deng, R. Xie, X. Ju, Z. Liu, L. Chu, Microfluidic Fabrication of Chitosan Microfibers with Controllable Internals from Tubular to Peapod-like Structures. *RSC Adv.* 2015, 5, 2, 928-936.

25 X. He, W. Wang, Y. Liu, M. Jiang, F. Wu, K. Deng, Z. Liu, X. Ju, R. Xie, L. Chu, Microfluidic Fabrication of Bio-Inspired Microfibers with Controllable Magnetic Spindle-Knots for 3D Assembly and Water Collection. *ACS Appl. Mater. Interfaces* 2015, 7, 31, 17471-17481.

26 J. Raven, P. Marmottant, F. Graner, Dry microfoams: Formation and Flow in a Confined Channel. *Eur. Phys. Jour. B* 2006, 51, 1, 137-143.

27 Y. Zhang, L. Wang, Experimental Investigation of Bubble Formation in a Microfluidic T-Shaped Junction. *Nanosc. Microsc. Therm.* 2009, 13, 4, 228-242.

28 M.T. Sullivan, H.A. Stone, The Role of Feedback in Microfluidic Flow-Focusing Devices. *Philos. Trans. A Math. Phys. Eng. Sci*. 2008, 366, 1873, 2131-2143.

29 C. Simpliciano, L. Clark, B. Asi, N. Chu, M. Mercado, S. Diaz,. M. Goedert, M. Mobed-Miremadi, Cross-Linked Alginate Film Pore Size Determination Using Atomic

Force Microscopy and Validation Using Diffusivity Determinations. *J. Surf. Eng. Mater. Adv. Technol.* 2013, 3, 4, 1-12.

30 Y.I. Yoon, H.S. Moon, W.S. Lyoo, T.S. Lee, W.H. Park, Superhydrophobicity of PHBV Fibrous Surface with Bead-on-String Structure. *J. Colloid Interface Sci.* 2008, 320, 1, 91-5.

31 N. Zhan, Y. Li, C. Zhang, Y. Song, H. Wang, L. Sun, Q. Yang, X. Hong, A novel Multinozzle Electrospinning Process for Preparing Superhydrophobic PS Films with Controllable Bead-on-String/Microfiber Morphology. *J. Colloid Interface Sci.* **2010**, 345, 2, 491-495.

32 X. Hong, M. Edirisinghe, S. Mahalingam, Beads, Beaded-Fibres and Fibres: Tailoring the Morphology of Poly(caprolactone) using Pressurised Gyration, *Mat. Sci. Eng. C - Mat. For Biolo. Appl.* 2016, **69**, 1373-1382.

33 H. Fong, I. Chun, D.H. Reneker, Beaded Nanofibers Formed During Electrospinning. *Polymers* 1999, 40, 16, 4585-4592.

34 N.E. Zander, Hierarchically Structured Electrospun Fibers. *Polymers* 2013, 5, 1, 19-44.

35 K. Maeda, H. Onoe, M. Takinoue, S. Takeuchi, Observation and Manipulation of a Capillary Jet in a Centrifuge-Based Droplet Shooting Device *Micromachines* **2015**, 6, 10, 1526-1533.

36 J.A. Champion, Y.K. Katare, S. Mitragotri, Particle shape: A New Design Parameter for Micro- and Nanoscale Drug Delivery Carriers. *J. Controlled Release* 2007, **121**(1-2), 3-9.

37 T. Nisisko, T. Ando, T. Hatsuzawa, Capillary-assisted abrication of biconcave polymeric microlenses from microfluidic ternary emulsion droplets. *Small* (*Weinheim an der Bergstrasse, Germany*) 2014, **10**(24), 5116-5125.

38 S.C. Glotzer, M.J. Solomon, Anisotropy of building blocks and their assembly into complex structures. *Nature materials* 2007, **6**(8), 557-562.

39 S. Sacanna, D.J. Pine, Shape-anisotropic colloids: Building blocks for complex assemblies. *Current Opinion in Colloid & Interface Science* 2011, **16**(2), 96-105.

40 S. Takka, F. Acarturk, Calcium alginate microparticles for oral administration: I: effect of sodium alginate type on drug release and drug entrapment efficiency. *J. microencapsulation* 1999, **16**(3), 275-290.

41 F. Acarturk, S. Takka, Calcium alginate microparticles for oral administration: II. effect of formulation factors on drug release and drug entrapment efficiency. *J. microencapsulation* 1999, **16**(3), pp. 291-301.

42 S. Takka, F. Acarturk, Calcium alginate microparticles for oral administration: III. The effect of crosslink agents and various additive polymers on drug release and drug entrapment efficiency. *Pharmazie* 1999, **54**(2), 137-139.

43 C. Qiu, M. Chen, H. Yan, H. Wu, Generation of uniformly sized alginate microparticles for cell encapsulation by using a soft-lithography approach. *Advanced Materials* 2007, **19**(12), 1603.

44 D. Dendukuri, D.C. Pregibon, J. Collins, T.A. Hatton, P.S. Doyle, Continuous-flow lithography for high-throughput microparticle synthesis. *Nature materials* 2006, **5**(5), pp. 365-369.

45 D. Baah, J. Tinger, K. Bean, N. Walker, B. Britton, T. Floyd-Smith, Microfluidic synthesis and post processing of non-spherical polymeric microparticles. *Microfluid. Nanofluid.* 2012, **12**(1-4), 657-662.

46 N. Hakimi, S.S. Tsai, C.H. Cheng, D.K. Hwang, One-step two-dimensional microfluidics-based synthesis of three-dimensional particles. *Advanced materials* (*Deerfield Beach, Fla.*) 2014, **26**(9), 1393-1398.

47 K. Liu, H.J. Ding, J. Liu, Y. Chen, X.Z. Zhao, Shape-controlled production of biodegradable calcium alginate gel microparticles using a novel microfluidic device. *Langmuir* 2006, **22**(22), 9453-9457.

48 Y.S. Lin, C.H. Yang, Y.Y. Hsu, C.L. Hsieh, Microfluidic synthesis of tail-shaped alginate microparticles using slow sedimentation. *Electrophoresis* 2013, **34**(3), 425-431.

49 T.D. Dang, S.W. Joo, Preparation of tadpole-shaped calcium alginate microparticles with sphericity control. *Colloids and surfaces.B, Biointerfaces* 2013, **102**, 766-771.

50 Y. Hu, G. Azadi, A.M. Ardekani, Microfluidic fabrication of shape-tunable alginate microgels: effect of size and impact velocity. *Carbohydrate Polymers* 2015, **120**, 38-45.

51 Y. Hu, Q. Wang, J. Wang, J. Zhu, H. Wang, Y. Yang, Shape controllable microgel particles prepared by microfluidic combining external ionic crosslinking. *Biomicrofluidics* 2012, **6**(2), 26502-265029.

52 Y. Hu, S. Wang, A. Abbaspourrad, A. M. Ardekani, Fabrication of shape controllable Janus alginate/pNIPAAm microgels via microfluidics technique and off-chip ionic cross-linking. *Langmuir,* 2015, **31**(6), 1885-1891.

53 D. N. Josephides, S. Sajjadi, Microfluidic method for creating monodisperse viscous single emulsions via core-shell templatingSource, *Microfluid. Nanofluid.,* 2015, 18, 383 -390.

54 J. Su, Y. Zheng, H. Wu, Generation of Alginate Microfibers with a Roller-assisted Microfluidic System, *Lab Chip* **2009**, 9, 7, 996-1001.

55 A. Greiner, J.H. Wendorff, Electrospinning: A Fascinating Method for the Preparation of Ultrathin Fibres. *Angew. Chem. Int. Ed.* **2007**, 46, 30, 5670-5703.

56 J. Huang, M. Juszkiewicz, W.H. de Jeu, E. Cerda, T. Emrick, N. Menon, T.P. Russell, Capillary Wrinkling of Floating Thin Polymer Films, *Science*, 2007, **317**, 650-653.

View Article Online
DOI: 10.1039/C8LC01081A

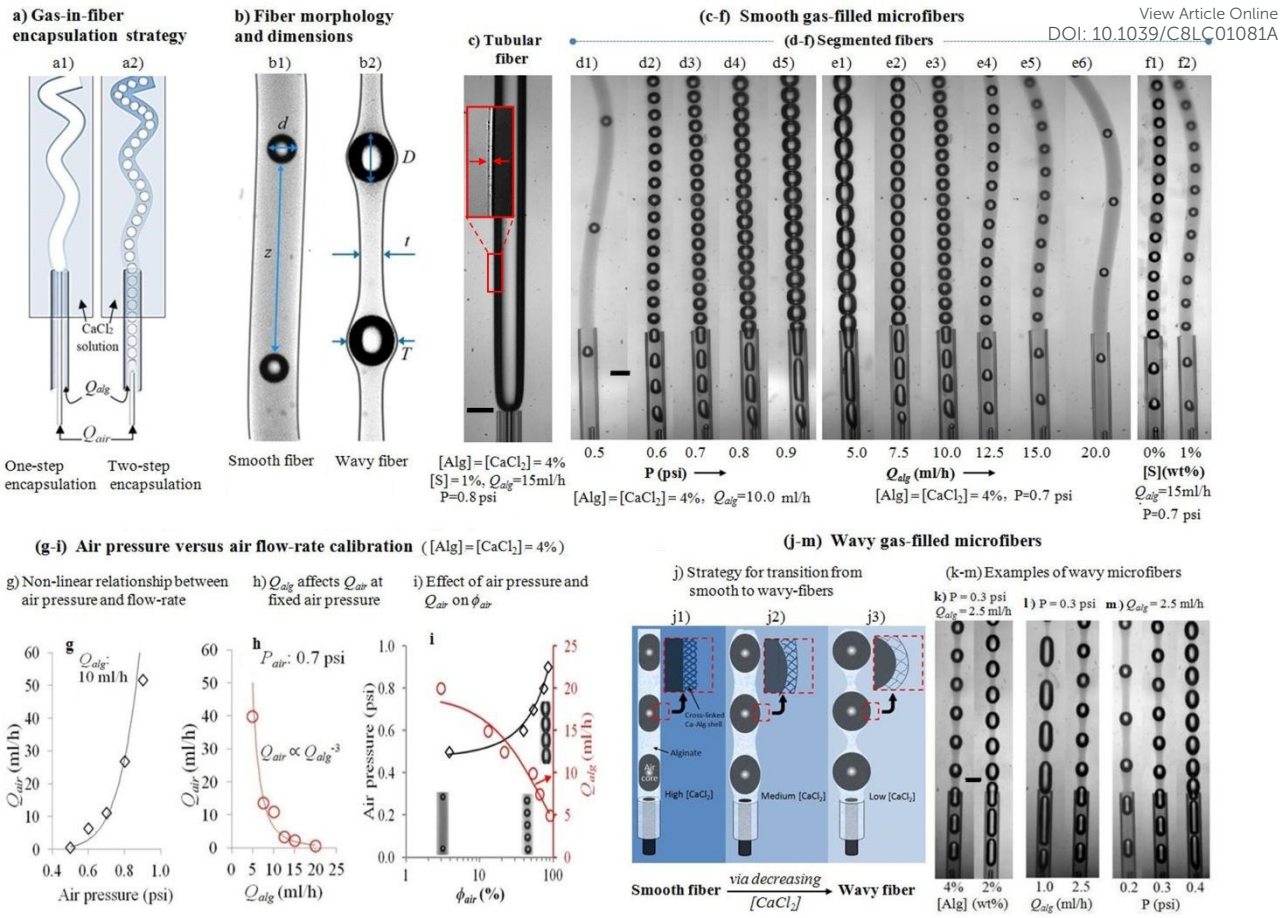

Fig. 1. (**a)** Schematics of *one-step* and *two-step* air-in-alginate microfluidic encapsulation approach. (**b)** Optical micrographs showing examples of fibers having smooth (b1) and wavy (b2) surface morphology in wet state, along with the illustration of assigned nomenclatures to fibers dimensions. **(c-f)** Tubular (c) and segmented (d-f) gas-filled microfibers, produced via *one-step* and *two-step* encapsulation techniques, respectively (common conditions were [Alg] = 4.0 wt% and [$CaCl_2$] = 4.0 wt%. Other conditions were P = 0.80 psi for (c), Q_{alg} =15 ml/h for (d), P = 0.80 psi for (e) and Q_{alg} =15 ml/h and P = 0.80 psi for (f). (d-f) represent the effects of increasing (d**)** air pressure, (e**)** alginate phase flow rate (Q_{alg}), and (f) surfactant concentration on the formation of smooth microfibers. **(g-i)** are **t**he variations in the air phase flow rate (Q_{air}) with (g) air pressure p and (h) Q_{alg}. (i**)** Represents the variations in internal phase ratio, or cavity ratio, of the fibers (φ_{air}) with air pressure (primary axis) and Q_{alg} (secondary axis). **(j-m)** Schematic representation (j) of formation of wavy bubble-filled microfibers in wet state via decreasing $CaCl_2$ concentration. (k-m) Examples of wavy air-encapsulated alginate microfibers made at [$CaCl_2$] = 1.0 wt% and [Alg] = 4.0 wt%. Effect of varying (k) alginate concentration, (l) Q_{alg}, and (m) air pressure (P) on the profile of wavy fibers. Other conditions are given above and under the photos. For all series [S] = 1.0 wt%, except for (f1).

View Article Online
DOI: 10.1039/C8LC01081A

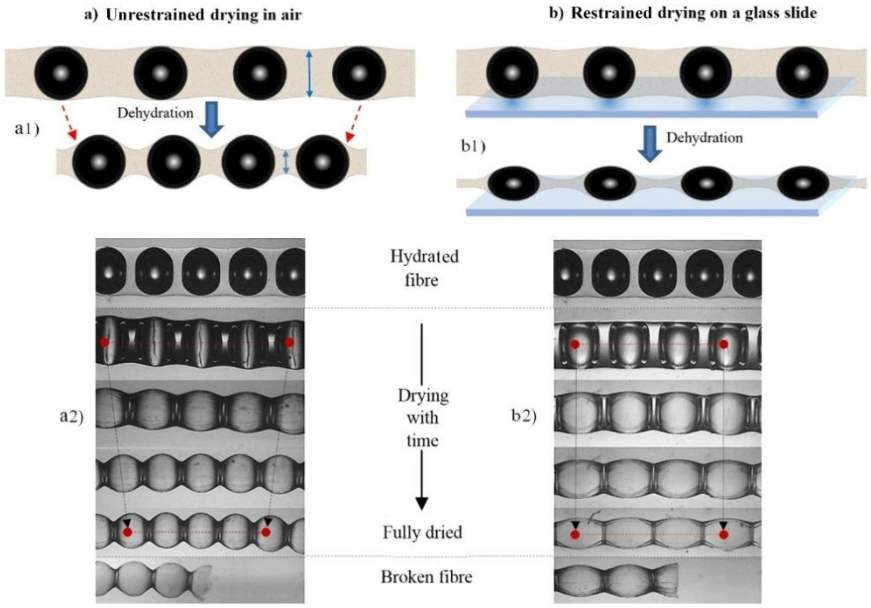

Fig. 2. a) Unrestrained drying versus **b)** restrained drying. Unstrained and restrained drying of air-encapsulated alginate microfibers are schematically illustrated in (a1) and (b1), respectively. The micrographs in (a2) and (b2) show the real-time variations in the morphology of a given fiber after unrestrained and restrained drying, respectively.

View Article Online
DOI: 10.1039/C8LC01081A

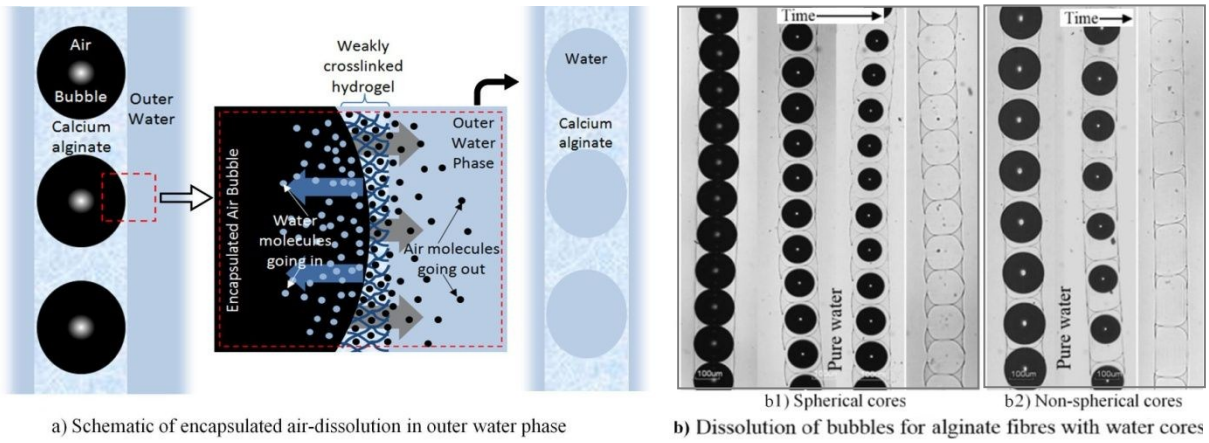

Figure 3. a) Schematic representation of dissolution mechanism of the encapsulated air bubble through a lowly cross-linked calcium alginate hydrogel shell, as depicted in the inset image. **b)** Real time monitoring of dissolution of (b1) spherical and (b2) non-spherical air-encapsulates within the fibers in pure water immediately after their formation in aqueous calcium chloride solution.

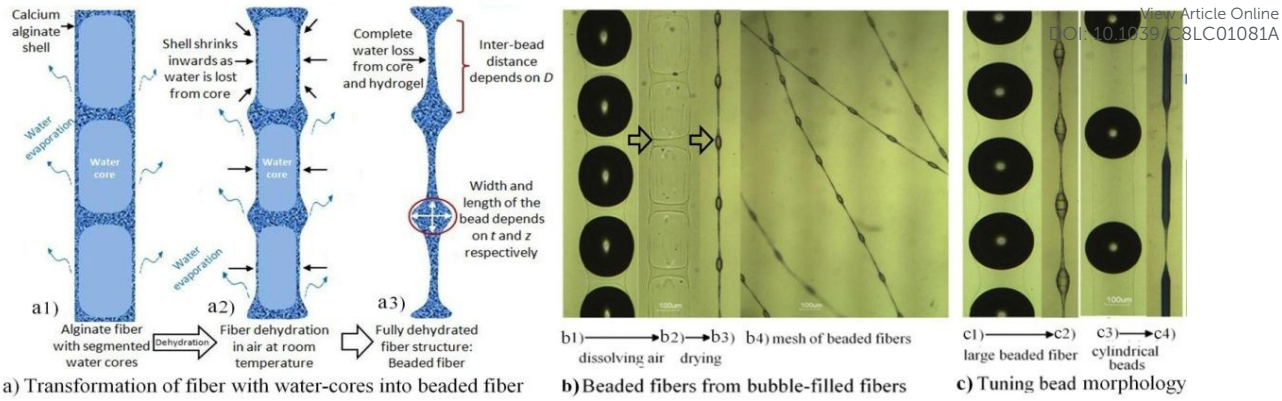

Figure 4. a) The schematic shows the evolution of fiber morphology during the transformation of a fiber with segmented water-cores into a beaded fiber via dehydration at room temperature. **b)** Microscopic images show a complete process for obtaining beaded fibers, where a bubbled fiber (b1) was first transformed into fibers with segmented water cores (b2) and then dehydrated to produce beaded alginate fibers (b3 and b4). **c)** The micrographs show two examples of how the size, shape and frequency of the beads were altered (c1→c2 and c3→c4).

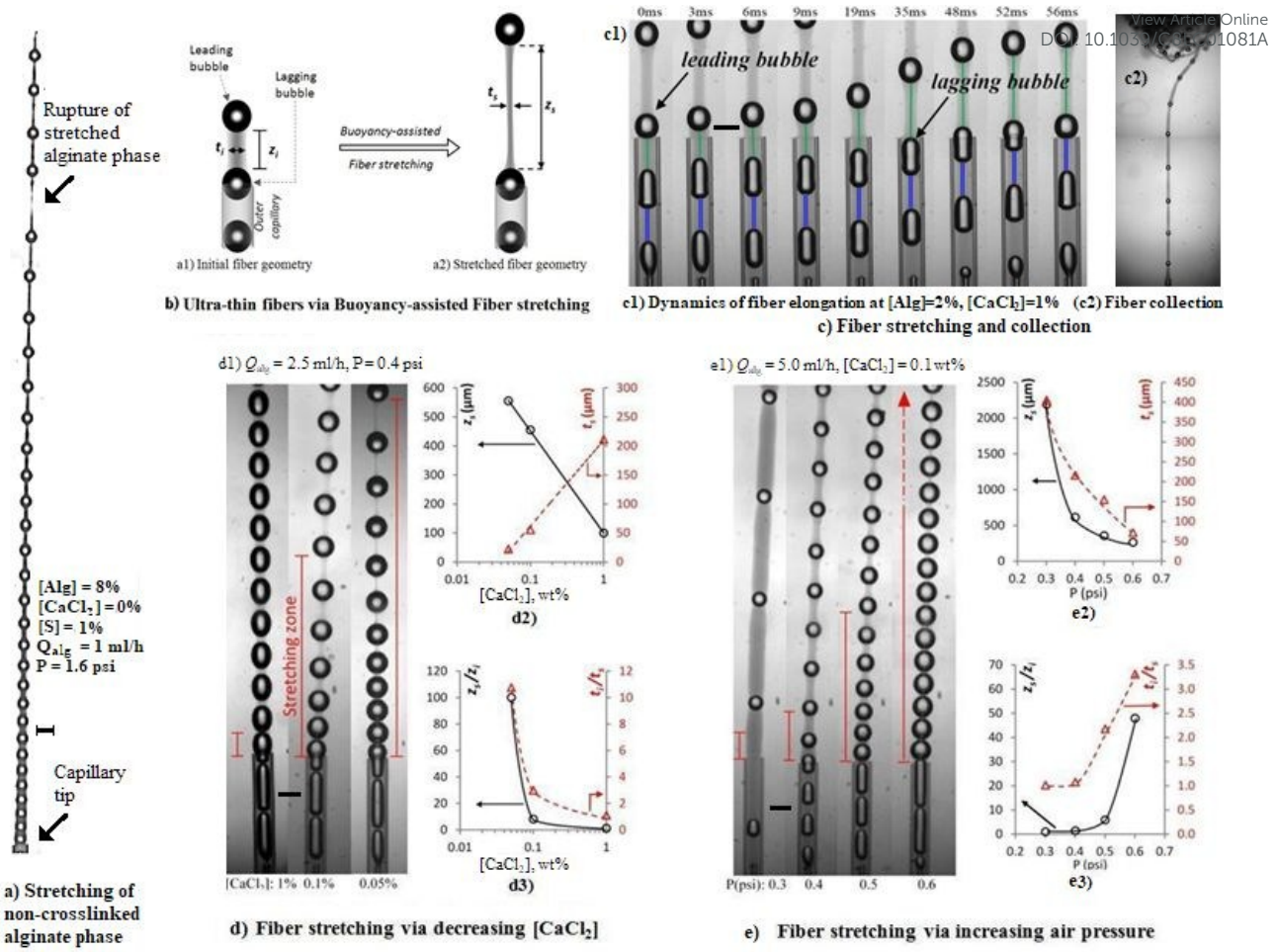

Fig. 5. a) The rupture of an alginate solution jet under the influence of buoyancy force in the absence of calcium chloride. **b)** Schematics show the initial fiber geometry just after exiting the outer capillary (a1), and the change in fiber geometry after it undergoes buoyancy-assisted stretching (a2). **c)** Time-evolution of fiber formation at low alginate and $CaCl_2$ concentration showing fiber elongation during formation ([Alg] = 2.0 wt% and [$CaCl_2$] = 1.0 wt%, P = 0.2 psi). c2) shows free-surface collection of the emerging threaded capsules. Formation of ultra-thin fibers via altering **d)** calcium chloride concentration, and **e)** air pressure, along with variations in stretched fiber thickness (t_s), fiber length (z_s), elongation (z_s/z_i) and thinning (t_i/t_s) factors. The red bars indicate the stretching zone (distance from the outer capillary tip, at which the stretching of the fibers stopped). The middle phase contained 4.0 wt% alginate. The scale bar is 400 μm.

View Article Online
DOI: 10.1039/C8LC01081A

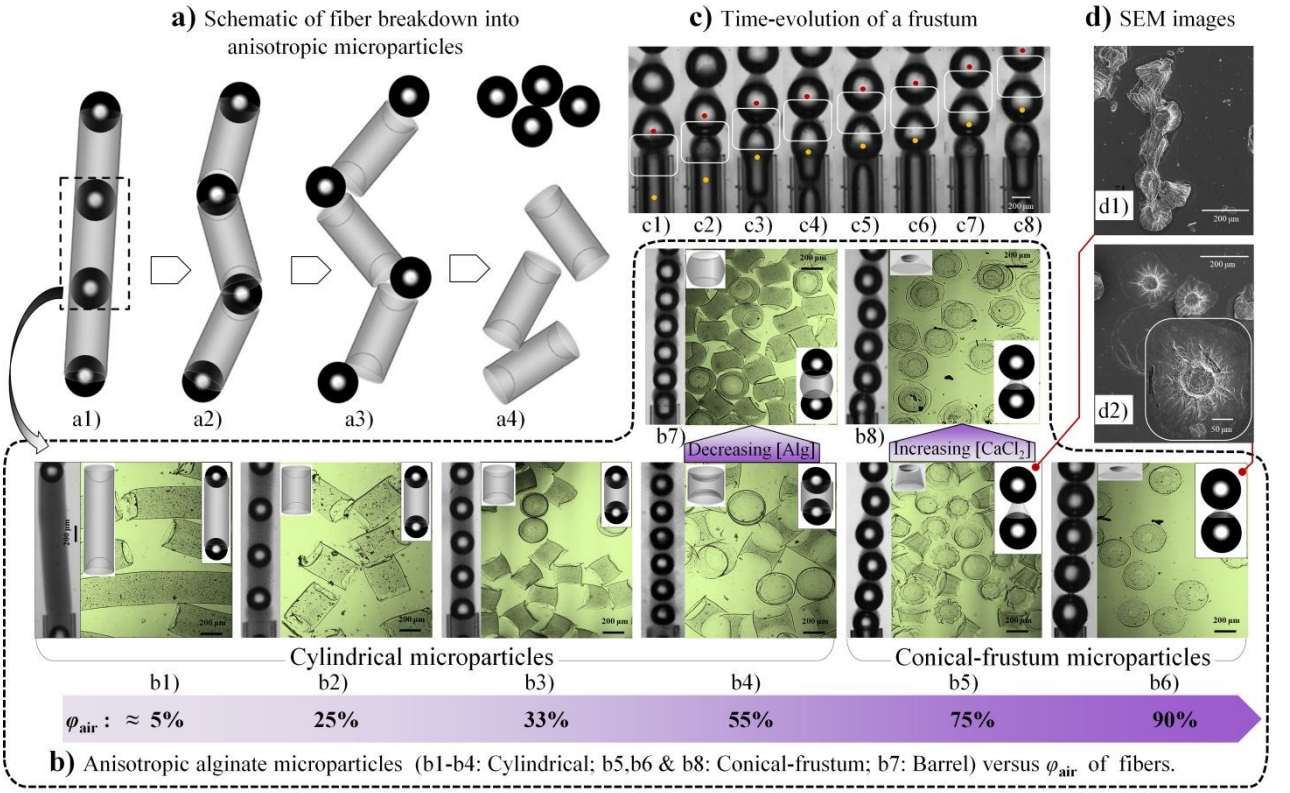

Fig.6. **(a)** Illustration of microparticle formation mechanism via controlled fiber destruction. **(b)** Micrographs of anisotropic microparticles formed with increasing φ_{air} (b1-b3) cylindrical-rods, (b4) ⧗ particle, (b5) conical-frustum, (b6) pact conical-frustum or plate (air pressure was 0.5, 0.6, 0.7, 0.8, 0.8 0.9, 1.1 psi for b1-b6, respectively; [S] = 0 wt%; [Alg] = 4.0 wt%; [$CaCl_2$] = 1.0 wt%; Q_{alg} = 5 ml/h except for b4 which was Q_{alg} = 8 ml/h). (b7) barrel microparticles formed at the condition of (b4) but using [Alg] = 2.0 wt%. (b8) thin conical-frustum formed at the conditions of (b5) but using [CaCl2] = 4.0 wt%. **(c)** Time evolution of a conical frustrum during formation. **(d)** SEM micrographs of conical-frustum microparticles formed; (d1) and (d2) correspond to (b5) and (b6), respectively. The insets on the right and left of images show corresponding formation of microfibers before break down, and a cartoon of the eventual shape of threads connecting the bubbles, respectively. The scale bar is 200 μm.

View Article Online
DOI: 10.1039/C8LC01081A

Table of content

The buoyancy force acting on fibers in a vertical microfluidic setup was utilized to form transformable air-filled hydrogel microfibers and microparticles.